Stipica Novoselac, Dražan Kozak, Todor Ergić, Darko Damjanović

FATIGUE DAMAGE ASSESSMENT OF BOLTED JOINT UNDER DIFFERENT PRELOAD FORCES AND VARIABLE AMPLITUDE ECCENTRIC FORCES FOR HIGH RELIABILITY

PROCENA ZAMORNOG OŠTEĆENJA VIJČANOG SPOJA POD DEJSTVOM RAZLIČITIH SILA PRITEZANJA I EKSCENTRIČNIH SILA S PROMENJIVOM AMPLITUDOM ZA VISOKU POUZDANOST

Abstract

Fatigue damage assessments of M10 bolted joint, made of 42CrMo4 heat treatable steel and strength class 10.9, were carried out for different preload forces and variable amplitude eccentric forces for high reliability. Assessments were done with preload forces of 50%, 70%, and 90% of force at bolt yield point and without preload force. The nominal approaches from Eurocode standard and VDI 2230 guidelines are mostly used for fatigue assessment. These nominal approaches cannot consider and describe in detail the local stress state at the thread root, which on bolt M10 have a radius of 217 μm. Threaded joints have several peculiarities that complicate the fatigue damage assessments. Range of dispersion is used to describe material cyclic scatter band with Gaussian normal distribution in logarithmic scales. Range of dispersion for notched structure of 42CrMo4 steel is taken from measurements. In order to take multiaxial stress field in thread root with high notch effect, multiaxial fatigue stress criterion based on a critical plane theory is applied for fatigue damage assessment. Critical plane approach is used for estimation of the fatigue damage and fatigue fracture plane position. Decrease of fatigue strength beyond the S-N curve knee point at $2 \cdot 10^6$ cycles is considered for the damage calculation. The main difficulties encountered in threaded joint fatigue damage assessment are due to the uncertainties and therefore, statistics and probability are applied. Assessments are carried out for 50%, 97.5%, 99%, 99.9%, 99.99%, 99.999%, 99.9999%, 99.99999%, and 99.999999% survival probability.

Izvod

Određivanje zamornog oštećenja M10 vijčanog spoja od toplotno obrađenog 42CrMo4 čelika, razreda čvrstoće 10.9, izvedeno je za različite sile pritezanja i ekscentrične sile promenjivih amplituda za visoke pouzdanosti. Istraživanje je sprovedeno sa silama pritezanja od 50%, 70%, i 90% sile na granici tečenja, kao i bez sile pritezanja. Nominalni pristupi prema normi Eurocode i VDI 2230 pravilniku se najčešće koriste za određivanje zamora. Nominalni pristupi ne mogu detaljno opisati lokalno stanje napona u korenu navoja, koji na vijku M10 ima radijus od 217 μm. Navojni spojevi sadrže nekoliko specifičnosti koje komplikuju određivanje zamornog oštećenja. Raspon rasipanja je korišćen za opisivanje rasipanja cikličkih svojstava materijala sa Gausovom normalnom raspodelom u logaritamskim koordinatama. Raspon rasipanja za konstrukciju sa zarezom od 42CrMo4 čelika preuzet je iz merenja. Da bi se uzelo višeosno stanje napona u korenu navoja s visokim uticajem zareza, višeosni zamorni kriterijum napona zasnovan na teoriji kritičnih ravni je primenjen za procenu zamornog oštećenja. Pristup sa kritičnim ravnima određuje zamorno oštećenje i poziciju zamorne prsline. Smanjenje dinamičke čvrstoće nakon $2 \cdot 10^6$ ciklusa na S-N krivoj uzeto je u obzir za proračun oštećenja. Glavne poteškoće određivanja zamornog oštećenja navojnog spoja su usled nesigurnosti i zbog toga su primenjene statistika i verovatnoća. Određivanje zamornog oštećenja izvršeno je za 50%, 97.5%, 99%, 99.9%, 99.99%, 99.999%, 99.9999%, 99.99999%, i 99.999999% verovatnoće preživljavanja.

INTRODUCTION

The high strength bolted joints are often used in a variety of industry. However, bolted joints can be damaged due to fatigue or hydrogen embrittlement (HE). Fatigue assessment of bolted joints are considered in fatigue problem areas and requires research /1, 2/. The problem of determining the threaded joints fatigue strength and damage has been investigated for many years. Fatigue limit affected by the stress gradients, size effect and surface quality for high reliability in industry are also in the problem areas. Off-shore and subsea applications where bolted joints are the critical points can be found on wellheads, xmas trees, drilling risers, structural connections, flanges, and similar /3, 4, 5/. Drill pipe threaded connections are susceptible to fatigue

damage because of high stress concentration due to the geometry and high mean stress induced by preload /4/. Fatigue life prediction using the Dang Van criterion for threaded joints was proposed on a drillstring joint used in the oil and gas industry /6/. The drillstring is a threaded assembly of tubes with a length of several kilometres, diameter of approximately 10–30 cm, and the roots radius of some millimetres /7/. For the oil and gas industry, Hill /7/ reported that 65% of the drillstring failures are related to fatigue problems. Fatigue of this problem is relevant /8, 9/. Therefore, high integrity of bolted joints are required. Although some recent work has investigated the fatigue of notched specimens /10-12/, the complete problem of the fatigue assessment procedure has not yet been solved. A similar work has also been presented in /13/ with bolt fatigue lifetime evaluation using Dang Van criterion. Investigations of the stress-gradient effect on fatigue have been performed using the Dang Van criterion /14, 15/. Development of deepwater reservoirs with higher water depths, higher pressure and higher temperature requires higher safety and reliability of structures /3/. It is well known that high strength steels are prone to HE and their resistance decreases with the strength increase. The resistance is generally expressed in terms of hardness limit above which the material is not recommended for use in the specific environment (e.g. sea water) or HE threshold stress intensity factors. Steels with yield strength below 800 MPa are generally resistant to HE /16, 17/. Design of bolted joints for offshore industry is governed by ASME Code: ASME B16.5 /18/ and API Standards: API 6A: Specifications for Wellhead and Christmas Tree Equipment /19/. The Health and Safety Executive from UK stated that the main cause of structural damage for installation in the North Sea is fatigue with 25%, whereas only 6% damage is due to corrosion /20/. Besides structures in oil and gas industry, automotive industry also has problems with bolted joints fatigue failures /21/, biomechanics with fatigue of pedicle screws used for spinal implants /22, 23/, and dental implants /24, 25/.

In order to assess the fatigue life of threaded joints on the basis of the nominal stresses, nominal approaches from standards Eurocode 3 /26/ and VDI 2230 guidelines /27/ are mainly used for fatigue assessment. However, bolted joints have a complex geometry with blunt notches and nonlinear contact interactions. The assessment methods based on nominal stresses cannot consider and describe in detail the local stress-strain state at the thread root. When assessment is done according to nominal approaches, without accurate thread notch dimensions, the definition of nominal stress is simple at first glance. For the bolted joint, it is average stress in the bolt cross-section calculated with simple engineering expressions or by FE analysis on ideally cylindrical bolt joint, usually without nonlinear contacts. At a closer look, the problems emerge due to many details and influence factors which are not taken into account. Even normal and fine threads are not different, so by engineering judgements distinction must be done. Variations within the thread details in dimensions and tolerances for thread roots and flanks, fatigue influencing factors, preload forces, and accurate stress distribution inside bolt continuum are not

covered. The consequence is that this reduction in details gives rise to the scatter of the fatigue assessments results, because even a change from normal to fine threaded joint can increase stress concentrations due to the smaller thread root radius. Investigation regarding the local strain approach is published, /28/.

Until recently, bolting technicians did not need to have the same competence standards as welders. However, in 2013 two standards were published highlighting the requirements for bolted joints. ASME updated the 2010 PCC-1 'Guidelines for Pressure Boundary Bolted Flange Joint Assembly' with an appendix defining the requirements for training and qualification of technicians working in the field of bolted joints. The European Committee for Standardization (CEN) re-published EN1591 Part 4 'Flanges and their Joints - Part 4: Qualification of personnel competency in assembly of the bolted connections of critical service pressurized systems'. Consequence of joint loosening result with fluid leakage and/or structure failure. Too low preload forces on dental implants can, for example, create microgap formation between dental implant and abutment screw which may foster bacterial invasion of the screw joint interface, /29/.

Load distribution and stresses in threaded joints have been widely investigated, /30-34/. All results show that load is not uniformly distributed along the threads and that the first engaged thread is subjected to the highest load. As observed by Croccolo et al. /35/, it is difficult to find in published investigations systematic and effective experiments concerning fatigue tests performed on screws or bolts. It is even more difficult to find investigations that take into account the tightened members, /36/.

Recent review by Patterson /37/ evaluated different methods for bolt fatigue life prediction. Even if the loading in the threaded joint is uniaxial, multiaxial (triaxial) stress state exists at the thread roots. Fatigue of the bolted joints requires a multiaxial fatigue criterion, /38/. Damage evaluation, without stress triaxiality consideration, results in an unrealistic fracture, /39/.

The state-of-the-art overview shows that the majority of approaches that estimate multiaxial fatigue behaviour in high-cycle fatigue (HCF) regime are either stress or energy quantities based on the critical plane approach /38-45/. The critical plane approach takes as a starting point that the fatigue damage reaches its maximum value on the plane of maximum shear stress amplitude τ_A /46-50/, and it is based on the hypothesis that stage I is the most critical stage in forming fatigue cracks. Furthermore, multiaxial fatigue strength is estimated with the stress perpendicular to the critical plane. The maximum normal stress (σ_{nmax}) relative to the plane with maximum shear stress amplitude (τ_A) is used to evaluate the detrimental effect of non-zero mean normal stress /46-50/. Therefore, according to the critical plane approach theory, fatigue damage depends on both τ_A and σ_{nmax}. Forsyth /51/ defined fatigue crack growth as a two stage process, where stage I corresponds to Mode II crack growth (caused by shear component) and stage II corresponds to Mode I crack growth (induced by normal components). This justified the use of both shear and

normal components in fatigue parameter definition, /52/. Fatigue strength depends not only on the value of the elastic stress but also on their spatial distribution because fatigue at a point is a nonlocal phenomenon, /53/. Detailed investigation of stress gradients influencing bolted joint fatigue behaviour is recently published, /54/.

The aim of this study is the fatigue damage assessment of M10 bolted joint, made of 42CrMo4 heat treatable steel, strength class 10.9, with different preload forces and variable amplitude eccentric forces for high reliability up to survival probability of P_S = 99.999999%. Range of dispersion is used to describe material cyclic scatter band with Gaussian normal distribution in logarithmic scales. This study takes into account elastic support from tightened steel members. Due to the high stress concentrations in thread roots, complex nonlinear contact interactions, complex loading combinations, and cyclic material nonlinearity, the stress gradient and critical plane approach based on stresses with multiaxial failure criterion are used for fatigue assessment. Decrease of fatigue strength beyond the S-N curve knee point at $2 \cdot 10^6$ cycles is considered for damage calculation according to the modified Palmgren-Miner linear damage accumulation hypothesis. Assessments are carried out for 50%, 97.5%, 99%, 99.9%, 99.99%, 99.999%, 99.9999%, 99.99999%, and 99.999999% survival probability.

MODELLING

Very detailed FE analyses are conducted to obtain the realistic stress distributions in the thread roots. FE model consists of: bolt, nut, and two plates, as shown in Fig. 1. Mesh is created with solid hexahedral elements (Abaqus C3D8 element) with 108332 nodes and 95652 elements. Thread profile is defined as axi-symmetric because it has been found that helical effect does not influence the load distribution, /55/. Nonlinear contacts are modelled with sliding surface contact. Contact surfaces are shown in Fig. 2a and 2b. Average finite element size in thread root is ≈ 30 μm. Experience suggests that average element size in thread root shall be within the interval 10-15% of thread root radius. In total, 4 element layers are created in depth with this size to accomplish a certain ratio. This ratio can be suggested as approximately 0.1-0.15% of bolt diameter (or any other threaded structure, for instance like drill pipe). In this case, result is ≈ 0.125 mm, as shown in Fig. 2c).

The coefficient of friction is set to $\mu = 0.1$. According to VDI 2230 Guidelines /27/, for material combination steel-steel in dry state, $\mu = 0.1$-0.23. Furthermore, according to VDI 2230 Guidelines, in the case of uncertainty about friction in the thread flanks and under the bolt head and nut, the lowest possible coefficient of friction must be selected. Preload scatter will be minimized if lubricants are used on thread contact surfaces. The bolted joint consists of M10 bolt, strength class 10.9 with metric standard thread (pitch according to DIN 13-1 and -28, stress cross section and cross section at minor diameter according to DIN 13-28, and minimum yield point according to DIN EN ISO 898-1).

Kinematic couplings are created in the middle of each plate for applying the eccentric forces and to hold the model.
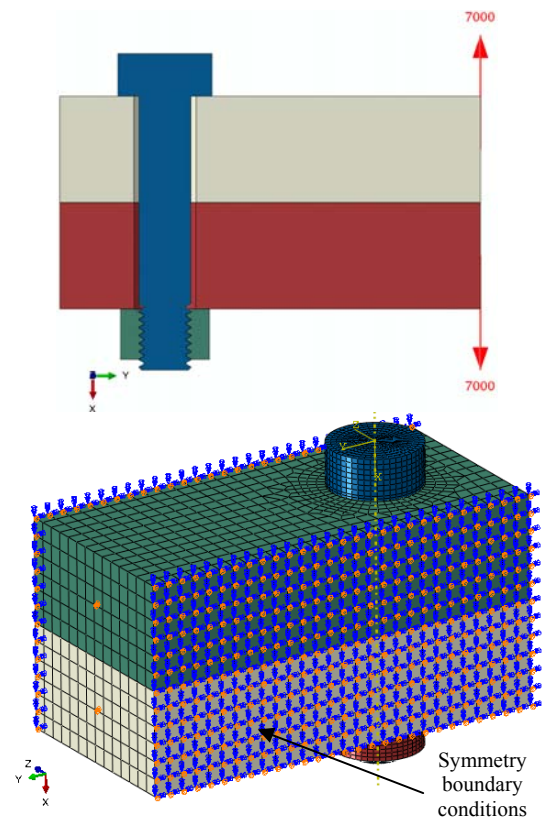

Figure 1. FE model of the bolted joint.
Slika 1. Model konačnih elemenata vijčanog spoja

Boundary conditions are defined around the plates with symmetry constraints in XY plane, and displacements in YZ direction on the kinematic couplings are prevented to establish a model without rigid body motion. During the in-service life of any bolted or threaded joint, first load is due to tightening. Bolt preload forces (F_p) are defined according to force at yield point ($F_{0.2}$) for M10 bolt, strength class 10.9, with value of $F_{0.2}$ = 55000 N, /27/. Applied preload forces are defined as 50, 70, 90, and 0% of $F_{0.2}$, and these forces define the models as 1, 2, 3, and 4, respectively. Abaqus command 'Bolt Preload' is used for application of the force on surface in middle of the bolt shank. In this case, there is only one bolt, but when there are more bolts, it is generally recommended to simultaneously introduce the tensioning of all bolts in-service, for instance in flange applications. In the case when only half of the bolts are tensioned simultaneously, elastic interactions between bolts occur which result in a small difference of preload forces in bolts, which can only be visible with ultrasonic or strain gauge measurements of tension in the bolts. After constant bolt preload force, further steps consist of additional eccentric forces with variable amplitudes, as shown in Fig. 3a. If only a proportion (normally 90%) of the minimum yield point $R_{p0,2min}$ of the bolt standardized according to DIN EN ISO 898-1 or DIN EN ISO 3506-1 may be utilized for the equivalent stress $\sigma_{eqv,Pall}$, then, with the utilization factor ν the equivalent stress due to the assembly preload force is:

$$\sigma_{eqv,Pall} = \nu R_{p0.2min} \qquad (1)$$

where ν is a utilization factor of the yield point stress (limit of full plastification of the cross section) during tightening.

a)

b)

c)

Average element size ≈ 30 μm

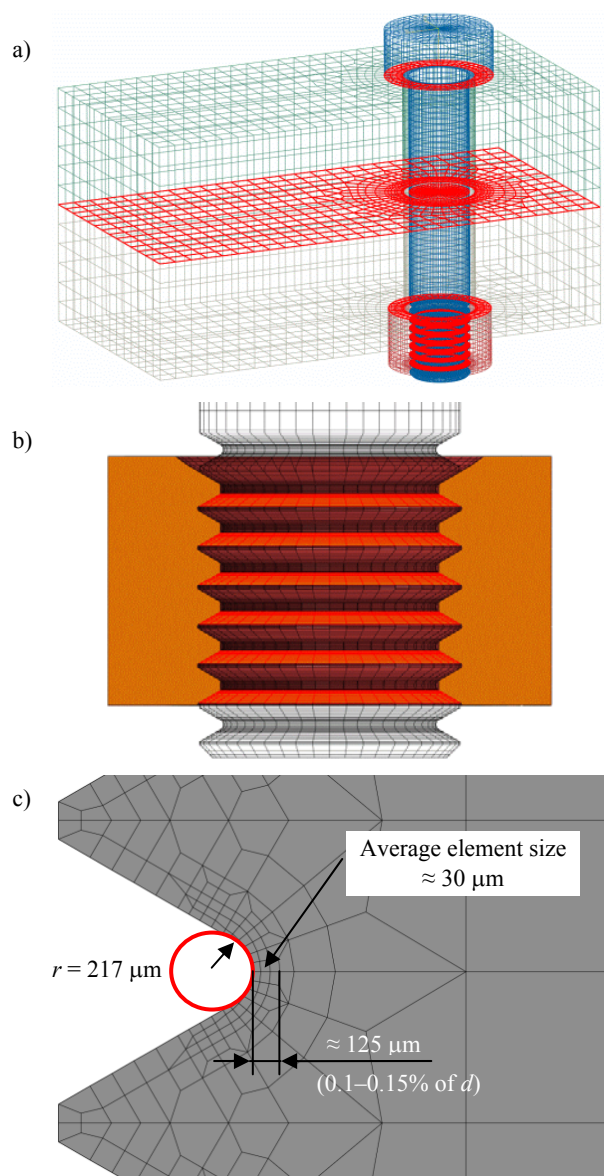$r = 217$ μm

≈ 125 μm
(0.1–0.15% of d)

Figure 2. (a) Contact surfaces; (b) detailed view of thread flank contacts; (c) mesh of thread root detail.
Slika 2. (a) Kontaktne površine; (b) detaljan pogled na kontakte bokova navoja; (c) pogled na mrežu detalja korena navoja

Allowable assembly stress can be calculated according to the following equation:

$$\sigma_{Pall} = \frac{\nu R_{p0.2min}}{\sqrt{1+3\left[\frac{3}{2}\frac{d_2}{d_0}\left(\frac{P}{\pi d_2}+1.155\mu_{Tmin}\right)\right]}} \quad (2)$$

where d_2 is pitch diameter of the bolt thread, d_0 is diameter at the relevant smallest cross section of the bolt, P is pitch, and μ_{Tmin} is minimal value of thread friction coefficient.

The allowable assembly preload force (F_{Pall}) may additionally be taken as 90% of the standardized minimum yield point ($R_{p0.2min}$) according to standard DIN EN ISO 898-1. Values from the standard have been calculated without taking into account dimensional and geometrical tolerances.

Cyclic eccentric tensile forces with variable amplitudes (FAE) are defined at 40 mm distance from bolt axis. Cumu-

lative spectrum distribution of variable amplitudes is shown in Fig. 3b. This type of block-program investigation is a Lo-Hi (Low–High) sequence, /56/.

Normal (F) and radial (F_r) force components on thread flank are shown in Fig. 4.
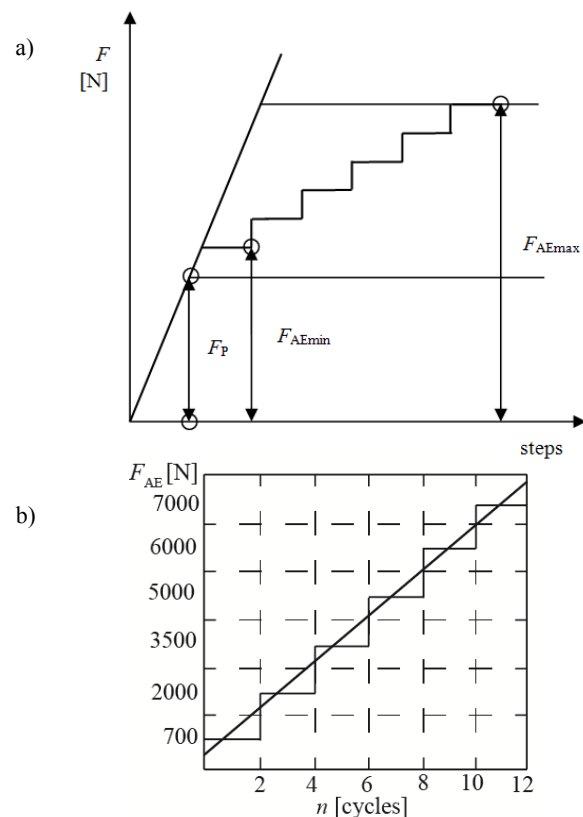
a)

b)

Figure 3. (a) Loadings on bolted joint; (b) Cumulative spectrum distribution of variable amplitudes.
Slika 3. (a) Opterećenja vijčanog spoja; (b) Raspodela spektra akumulacije promenjivih amplituda
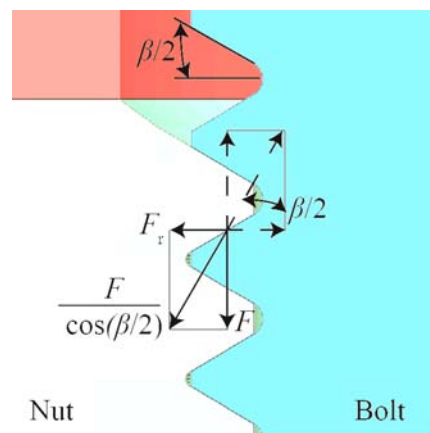

Figure 4. Force components on thread flank.
Slika 4. Komponente sile na bokovima navoja

Equivalent stresses in bolts are usually calculated according to the VDI 2230 with following the equation:

$$\sigma_{\perp eqv} = \sqrt{(\sigma_{\perp max})^2 + 3(k_{\perp \tau}\tau_{\perp t})^2} \quad (3)$$

where σ_{max} is maximal tensile stress, $\sigma_{max} = F_{Smax}/A_0$, where $A_0 = A_S$. A_S is the bolt stress section. τ_t is the maximal shear

stress. k_τ is a reduction coefficient for shear stress during the life. Usually, $k_\tau = 0.5$ /27/.

Numerical analyses are done on FEM model in Abaqus 6.12 (Simulia, Providence, RI, USA). The stress tensors with influence factors and nonlinear cyclic material properties are further calculated in the FemFat 4.8 (ECS, Steyr, Austria) software.

42CrMo4 HEAT TREATABLE STEEL PROPERTIES

For bolt strength grade 10.9, the frequently used material is 42CrMo4, /57/. Alloy steels, mainly 42CrMo4, 40NiCrMo6, and 34CrNiMo6 remains the most common material for subsea fasteners, /3/.

Material monotonic and cyclic properties are shown in Table 1. According to DIN EN 10 083-1 this material is in the class of heat treatable steel, /58/. Cyclic stress-strain hysteresis loop behaviour is defined with cyclic coefficient of hardening $K' = 1.61 \cdot R_m$ and cyclic exponent of hardening $n' = 0.15$ /56, 59/.

Smooth circular specimen diameter for basic material cyclic properties is 7.5 mm. The S-N curve for alternating

Table 1. Monotonic and cyclic properties for 42CrMo4 steel
Tabela 1. Monotona i ciklična svojstva čelika 42CrMo4.

Property	Value
Modulus of elasticity, E [MPa]	210000
Poisson coefficient, ν [-]	0.3
Tensile strength, R_m [MPa]	1100
Yield strength, $R_{0.2}$ [MPa]	900
Cyclic coefficient of hardening, K' [MPa]	1771
Cyclic exponent of hardening, n' [-]	0.15
Elongation at fracture, A [%]	11

tension/compression loading (stress ratio $R = -1$) and relative stress gradient ($\chi' = 0$) with survival probability defined at 50% is shown in Fig. 5a. The fatigue limit for $R = -1$ have a knee-point in the S-N curve at $2 \cdot 10^6$ cycles with the slope of $k = 12$. Alternating fatigue strength under tension/compression ($R = -1$) is $\sigma_{D,tc} = 495$ MPa /58/. Due to the issues of uncertainty, material cyclic properties uncertainties in the S-N curve are considered in this investigation and reliability is taken into account. The concept of fatigue reliability is illustrated schematically in Fig.5a. The equation of the S-N curve (for $R = $ const.):
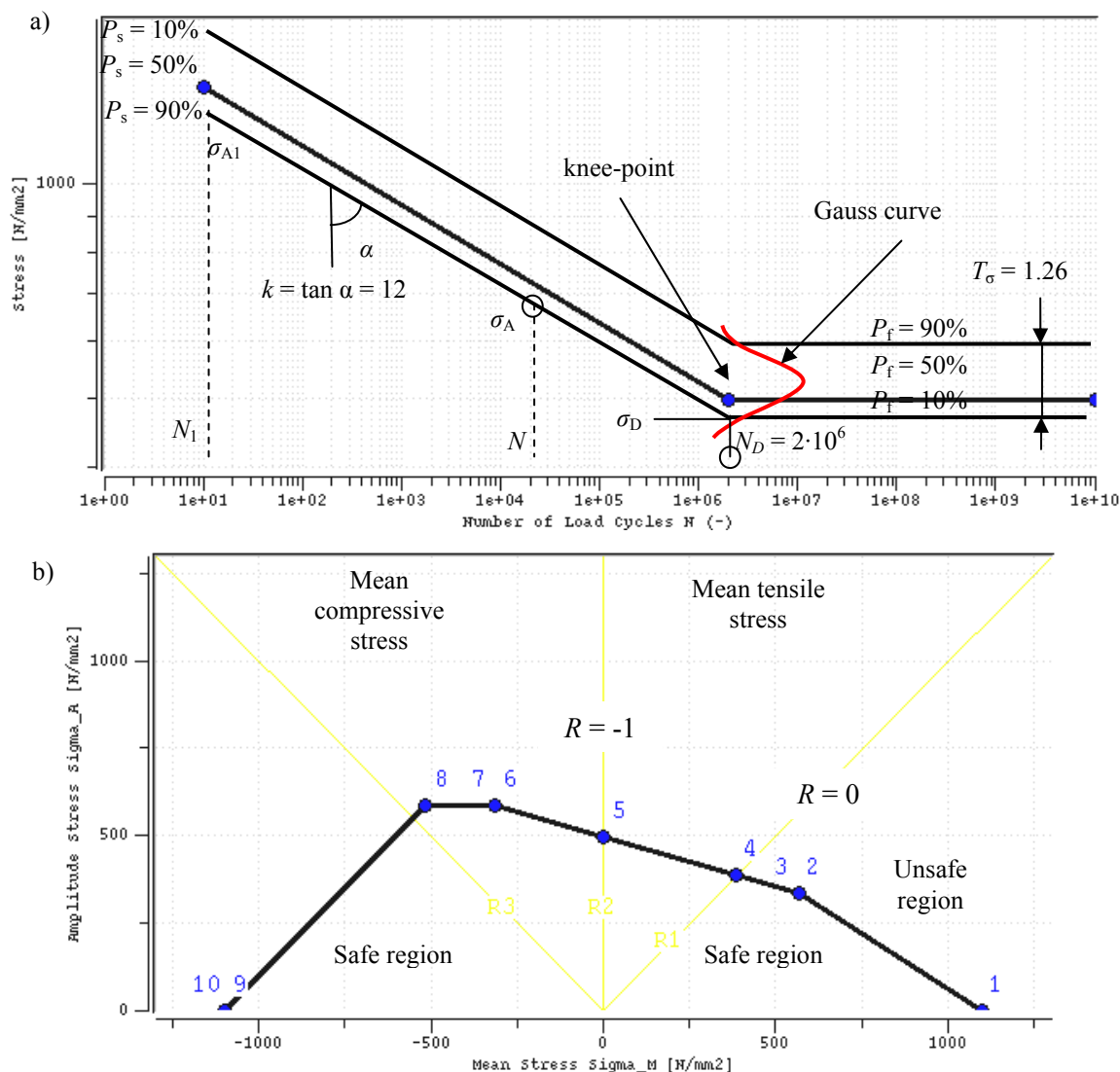

Figure 5. 42CrMo4 steel: a) S-N curve; and b) Haigh diagram.
Slika 5. 42CrMo4 čelik: a) S-N kriva i b) Hejgov dijagram

$$\sigma_A = \sigma_D \left(\frac{N_D}{N} \right)^{1/k} \tag{4}$$

$$k = \tan\alpha = \frac{\Delta(\log N)}{\Delta(\log \sigma_A)} = \frac{\log(N_1/N_2)}{\log(\sigma_{A1}/\sigma_{A2})} \tag{5}$$

Mean stress influence is taken into account by means of the Haigh diagram, which is generated by polygonal lines. Fatigue strength is decreased for tensile mean stress and increased for compressive mean stress. Therefore, Haigh diagram is unsymmetrical, as shown in Fig. 5b. Mean stress rearrangement is done according to the Neuber-hyperbola with FemFat PLAST.

FATIGUE DAMAGE CALCULATION

The calculation of local S-N curve and Haigh diagram starts from the known basic smooth specimen data, as was explained in previous chapter. At each node the particular local S-N curve and Haigh diagram is calculated from the specimen cyclic fatigue properties, influence factors, and stress conditions. The definition of the S-N curve model in the double logarithmic system is that the linear damage accumulation is done with the amplitude stress tensor of the particular hysteresis. Other influences like stress distribution, notch effects, diameter, mean stress, mean stress rearrangement due to local plastification, surface roughness and statistics (range of dispersion and survival probability) are taken into account at a locally modified S-N curve and Haigh diagram to obtain correct endurance fatigue limit at critical areas. Transfer of the results from specimens to components is one of the main challenges for fatigue assessment, /60/. The main purpose of the equivalent stress calculation algorithm is reduction of the multiaxial (triaxial) stress state in the thread roots to the equivalent uniaxial state with a criterion of multiaxial fatigue failure, suitable for a given ductile material. After that, the calculated equivalent stress history is processed in order to make assessment of the fatigue life. Loading history is analysed in the time domain with the numerical algorithm of Rainflow cycle counting. The critical plane position is determined with damage accumulation method /59, 61-66/. Fatigue fracture plane is defined by its orthogonal vector according to the following equation:

$$\vec{\eta} = \hat{l}_1 \vec{i} + \hat{m}_1 \vec{j} + \hat{n}_1 \vec{k} \tag{6}$$

where $\vec{i}$, $\vec{j}$, and $\vec{k}$ are unit normal vectors of critical cutting plane along the axes x, y, and z, respectively. Furthermore, $\hat{l}_1$, $\hat{m}_1$, and $\hat{n}_1$ are direction cosines of the principal stresses referred to a coordinate system (x, y, z). The normal stress at every time point $\sigma_\eta(t)$ acting on this fatigue fracture plane is given by /67, 68/:

$$\sigma_\eta(t) = \hat{l}_1^2 \sigma_{xx}(t) + \hat{m}_1^2 \sigma_{yy}(t) + \hat{n}_1^2 \sigma_{zz}(t) + \\ + 2\hat{l}_1 \hat{m}_1 \tau_{xy}(t) + 2\hat{l}_1 \hat{n}_1 \tau_{xz}(t) + 2\hat{m}_1 \hat{n}_1 \tau_{yz}(t) \tag{7}$$

For each cutting plane, which is defined by its orthogonal vector $\vec{\eta}$, Eq.(6), the orthogonal and the shear stress components are determined separately for the mean stress and the stress amplitude tensor. Therefore, the stress com-ponents normal to the cutting plane are stress amplitudes and mean stress at every time point.

Equivalent stress algorithm used for the fatigue damage is scaled normal stress in critical plane. This algorithm solves the problem of identifying closed stress cycles for complex random loads with spatial stress states and rotary normal stresses. This algorithm is recommended for ductile materials, /59/. This algorithm takes into account the damaging effect of shear. Damage equivalent scaling of normal stress in material planes is dependent on the stress state (tension/compression, shear, hydrostatic stress state, and its combinations). A variable, $V(t_i)$ is introduced to characterize the stress state at each time step t_i. The first step in the stress algorithm is calculation of principal normal stress $\sigma_1 > \sigma_2 > \sigma_3$ at every time point. Furthermore, the variable $V(t_i)$ represents the ratio between the minimum and maximum principal normal stress in time and is calculated according to the following equations:

$$V(t_i) = \frac{\sigma_3}{\sigma_1} \quad \text{for} \quad |\sigma_1| > |\sigma_2| \tag{8}$$

$$V(t_i) = \frac{\sigma_1}{\sigma_3} \quad \text{for} \quad |\sigma_2| > |\sigma_1| \tag{9}$$

Ratio V can be between −1 and +1. Certain ratios represent three different stress states:
- $V(t_i) = -1$ for dominant shear load,
- $V(t_i) = 0$ for dominant tension/compression load,
- $V(t_i) = 1$ for hydrostatic stress state.

Mohr's circle of stress states for torsion, uniaxial tension, and hydrostatic loading are shown in Fig. 6, respectively.
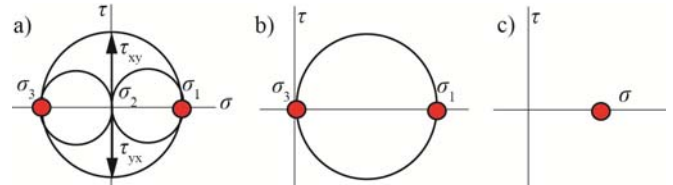

Figure 6. Mohr's circle of stress for: a) torsion, b) uniaxial tension, and c) hydrostatic loading.
Slika 6. Morov krug napona za: a) torziju, b) jednoosno zatezanje i c) hidrostatičko opterećenje

Moreover, the stress tensor in time is scaled as a function of $V(t_i)$. The scaling factor is calculated according to the:

$$f(t_i) = 1 + (1 - k)\, V(t_i) \tag{10}$$

where k is a material ductility factor, which can be calculated according to the following equation:

$$k = \frac{\sigma_D}{\tau_D} \tag{11}$$

where σ_D and τ_D are alternating and shear fatigue limit, in respect. With this approach, stress is not modified for tension/compression. For dominant shear it is scaled up by the factor k, in order to model the damaging effect of shear /68/. For the hydrostatic stress state, $f(t_i)$ is linearly extrapolated. Therefore, the magnitude of the hydrostatic stress is scaled down which correlates with the distortion energy criterion. This algorithm can be used to solve biaxial and triaxial stress states, /68/. With the critical cutting plane

method, the normal stress in the cutting planes is scaled with $f(t_i)$ for each time point.

The damage accumulation method includes accumulation of fatigue damage on all critical planes. Furthermore, the plane of the maximum damage degree is selected as the most critical. Multiaxial interaction between stress amplitude tensors and mean stress tensors is solved with critical plane approach in combination with the Haigh diagram. If in the cumulative loading spectrum with variable amplitude of a bolted structure the local stress values are in the elastoplastic area of material, then the mean stress tensors are rearranged by means of Neuber-hyperbola rule in the cycle stabilised stress-strain curve. The Haigh diagram is used to define the most critical cutting plane angle and the damaging factor for each node. Cutting plane is defined at every 10°. The relative stress gradient (χ') influences the local S-N curve (both slope k and endurance cycle limit N_D), and fatigue strength limit σ_D. Mean stress and surface roughness influence also the local S-N curve, and fatigue strength σ_D, whereas influence factors as size and statistics influence only fatigue strength σ_D.

The modified Palmgren-Miner linear damage accumulation (or sometimes called Haibach) hypothesis is used for the evaluation of fatigue life. The fatigue damage accumulation is calculated from Eq.(12):

$$D = \sum_{i=1}^{n} \frac{n_i}{N_i} \quad (12)$$

where n_i is the number of applied certain stress amplitudes and N_i is number of cycles to failure at that certain stress.

The drop of fatigue strength in the high-cycle range is considered using S-N curve for the damage calculation with fictitious slopes beyond the knee point of $k' = 2k – 1$ or $2k – 2$ (according to Haibach, /56/) depending on material condition (wrought, cast or welded). In engineering standards the knee point of the S-N curve is defined as the transition to infinite life. Recent experimental results up to giga-cycles show that there is a further decline of the S-N curve beyond the knee point at higher cycles. The fatigue strength decline of ≈ 10% per decade is usually assumed. The S-N curve is generally limited to 10^6, $2\cdot10^6$, $5\cdot10^6$, 10^7 cycles or some other value depending on the standard or structure, /69/. Beyond knee point, it is considered that the fatigue life is infinite. In principle, the fatigue limit is given for a particular number of cycles to failure. Fatigue limit is given by the average alternating stress σ_D and the probability of fracture is given by the standard deviation of scatter (s). There is no knee point between 10^6 and 10^9 cycles for the Cr-Mo steel as the fatigue limit σ_D decreases by 60 MPa, /69/. Various standards and regulations point out /58, 26, 70/ that the fatigue limit does not exist in the case of jointed components such as press-fits or bolted joints because of fretting, high temperature, and/or corrosion, /71/.

From the resulting equivalent stress history, a Rainflow cycle counting is applied to identify closed cycles in the stress-strain-path. This basically means that the resultant loading is saved in a square 64×64 amplitude/mean stress matrix. Rainflow counting method has been shown to be a superior method compared with peak, range and the range-pair method, /72/. Rainflow cycle counting method is first proposed by Endo in 1971, /73/. The counting method is described in an ASTM standard, /74/.

The multiaxial fatigue criteria is based on the fatigue crack initiation stage and the fatigue crack growth stage is not included. The bolt thread surface roughness is defined as $R_z = 2.5$ μm. Influence of size is also taken into account in accordance with FKM-Guidelines, /58/, with the bolt diameter of 10 mm. It has been found that the fatigue life reduces as the bolt nominal size increases, /57/.

Instead of the standard deviation s, common in statistics, fatigue testing and analysis usually use the range of dispersion. The range of dispersion for cyclic material properties is defined as the ratio of the bolt fatigue strength at 10% survival probability to fatigue strength at 90% survival probability P_S.

$$T_S = 1 : \frac{\sigma_D(P_S = 10\%)}{\sigma_D(P_S = 90\%)} \quad (13)$$

The following simple relationship exists between cycle range of dispersion T_N and T_S, where k is included as the slope of the S-N curve:

$$T_N = T_S^k \quad (14)$$

For example, a value of $T_S = 1.5$ (after Radaj) may be specified for analysing a welded joint in structural steel.

In statistics, a Gaussian distribution is described by the mean value and the standard deviation. The statistics applied regarding distribution type is the Gaussian Log-Normal distribution for calculation of statistics influencing variables, both for range of dispersion and survival probability. The characteristic parameters of the scatter band are the standard deviations s_σ and s_N relating to σ_A and N, respectively and alternatively, they are related to the T_S and T_N. The logarithmic standard deviation s and the T_S are related by equations:

$$s_\sigma = \left(\frac{1}{2\cdot1.28}\right)\log\left(\frac{1}{T_S}\right) \quad (15)$$

$$s_N = \left(\frac{1}{2\cdot1.28}\right)\log\left(\frac{1}{T_N}\right) \quad (16)$$

Range of dispersion for notched structure of 42CrMo4 quenched and tempered steel is taken from measurements, /75/. From measurements of 300 smooth specimens ($K_t = 1$) made of 42CrMo4 steel at $R = –1$ and $R = 0$, it is obtained that $T_S = 1.12$. However, from measurements of 372 notched specimens (with maximal $K_t = 5.2$) made of 42CrMo4 quenched and tempered steel at $R = –1$ and $R = 0$, it is obtained that $T_S = 1.26$. For 18 specimens under alternating bending with $K_t = 1.6$ and 25 specimens under alternating torsion with $K_t = 1.35$, obtained range of dispersion is again $T_S = 1.26$. From these measurements, it is obvious that stress concentration lead to higher range of dispersion. This value is additionally also recommended for steel in /68/. Therefore, range of dispersion is set as $T_S = 1.26$. It is interesting to compare the range of dispersion distribution under normal stresses for stress relieved welded joints of $T_S = 1.55$ for $R = 0.4$, $T_S = 1.42$ for $R = 0$, and $T_S = 1.44$ for $R = –1$, /76/. From results published in /77/ for welded

joints of high-strength steels under axial and bending constant amplitude loadings, obtained range of dispersion is $T_S = 1.50$. For laser beam welded thin-sheet steels and aluminium alloys ($t = 1$–2 mm), results are $T_S = 1.30$ and $T_S = 1.36$, respectively, after Eibl et al. /78, 79/.

The fatigue strength of a bolted joint depends on the notch effect which contains both stress concentration and strength reduction by notches. High stress gradients resulting from stress concentrations in thread roots by bending of the bolt and thread flanks cause the material surface to be supported with micro support effect, which results in higher surface fatigue strength, /54/. Gradient support effect is determined with the relative stress gradient (χ'). Furthermore, support effects are evaluated with the FemFat method /59/. According to this method, the ratio of cyclic tensile/compressive strength to the bending fatigue strength can be used to calculate the support factor n:

$$n = f_{GR,af} = 1 + \frac{(\sigma_{A,b}/\sigma_{A,tsc}) - 1}{(2/b)^v} \chi'^v \qquad (17)$$

where $\sigma_{A,b}$ is the material alternating stress limit for bending and $\sigma_{A,tsc}$ the material alternating stress limit for tension/compression. The material parameter v takes into consideration the nonproportional increase in the support effect with regard to the relative stress gradient. For steel, $v = 0.3$ /59/. Specimen thickness is b. Factor $f_{GR,af}$ is the stress gradient factor influencing the fatigue limit. The influence of the χ' on the slope $k_{C,GR}$ of the local component S-N curve is calculated with the following equations:

$$f_{GR,af} = 1 + \frac{1.8 \cdot \chi'^1 \cdot 2}{f_{GR,af}} \chi'^v \qquad (18)$$

$$k_{C,GR} = \frac{(k_M - IFK2)}{f_{GR,sf}^{IFK3}} + IFK2 \qquad (19)$$

where $f_{GR,sf}$ is the stress gradient influence factor affecting the slope of the local component S-N curve; $k_{C,GR}$ is the slope of the local component S-N curve as a result from the gradient influence, k_M is the slope of the material S-N curve at $R = -1$, $IFK2$ is the slope exponent of the specimen fracture S-N curve, $IFK3$ is the material class dependent exponent (for the steel, $IFK2 = 3$ and $IFK3 = 2$, /59/).

RESULTS

Fatigue damage assessments are carried out for following survival probabilities P_S: 50%, 97.5%, 99%, 99.9%, 99.99%, 99.999%, 99.9999%, 99.99999%, and 99.999999% for 4 numerical models. Stress distributions for model 1 are shown in Fig. 7. Detailed views on threaded region with section cut in xy plane clearly shows Max principal, Min principal, shear τ_{xy}, and Tresca stress distribution after tightening with 50% of $F_{0.2}$ and variable amplitude loadings. Stresses are shown for step with maximal eccentric tensile forces. The deformation scale in figures is set to 10. Maximal values of all shown stresses are on the first engaged thread root. High stress values are present in the model due to the liner-elastic material definition, which lead to the usage of Neuber-hyperbola for achieving realistic elastic-plastic behaviour.

The fatigue damage distribution in the thread roots reveals that the first 3 thread roots have the highest damage, whereas the first engaged thread has maximal damage, as can be observed from Fig. 8a and b. The results are shown for model 2 (with 70% of $F_{0.2}$) for $P_S = 99.9999\%$. Furthermore, stress amplitudes are shown in Fig. 8c and d. The results show that maximal stress amplitude of $\sigma_A = 93$ MPa is obtained at the first engaged thread root.

It is a well known fact that, at thread roots, very high stress concentrations occur and under preload force significant mean stresses are introduced in roots. These high mean stresses are introduced in thread roots due to preload force and together with the stress amplitudes under dynamic loadings govern the fatigue performance.

The fatigue damage assessments for all 4 models and for all survival probabilities are shown in the following tables. Tables show fatigue damage and fatigue limit for model 1 (with 50% of $F_{0.2}$), model 2 (with 70% of $F_{0.2}$), model 3 (with 90% of $F_{0.2}$), and model 4 (with 0% of $F_{0.2}$), respectively. The results are shown for most critical node in first engaged thread root where highest damage is obtained. Model 1 has a highest damage of $D = 2.53E\text{-}06$ and fatigue limit of $\sigma_D = 179$ MPa for $P_S = 99.999999\%$. Further increase of bolt preload force F_P leads to a lower fatigue damage. For instance, model 3 has a highest damage of $D = 100.97E\text{-}09$. However, with increase of F_P, fatigue limit is decreased. On the other hand, with increase of F_P, maximal stress amplitude decreases. For instance, model 1 with 50% of $F_{0.2}$, which results with $F_P = 27500$ N, has a $\sigma_A = 232$ MPa, whereas model 3 with $F_P = 49500$ N results with $\sigma_A = 58$ MPa. Present results show that model 4 (without the preload force) has the highest fatigue damage. Maximal damages are in all cases always for $P_S = 99.999999\%$, as expected. One of the main and biggest challenges for fatigue assessment is how to transfer the results from specimens to components /60/. In this particular case of threaded joint, the problem is how to transfer the results from smooth circular specimen to the threaded region. Specimens have alternating fatigue limit of $\sigma_{D,tc} = 495$ MPa for tension/compression ($R = -1$), for alternating bending $\sigma_{D,b} = 525$ MPa, and for alternating shear $\tau_D = 285$ MPa, /58/. It is evident that the calculated fatigue limit strongly depends on preload force. Fatigue limit is highest for $F_P = 0$ N with value of $\sigma_D = 480$ MPa. Lowest fatigue limit is calculated for $F_P = 49500$ N with value of $\sigma_D = 193$ MPa. It is interesting to observe the decrease of the fatigue limit from $P_S = 50\%$ to 99.999999%. Decrease of 76 MPa is calculated for $F_P = 49500$ N, whereas 191 MPa for $F_P = 0$ N. The diagram in Fig. 9 makes it evident that σ_D has a significant decrease for lower failure probabilities. From this diagram, it can be easily seen that curves have a shape of Gaussian distribution.

The unit vectors of critical cutting plane for crack initiation are shown in Fig. 10a, b and c. The unit normal vectors of critical cutting plane $\vec{i}$, $\vec{j}$, and $\vec{k}$ are related to the axes x, y, and z, respectively. As can be seen from these figures, unit normal vector $\vec{i} = 0.9848$, $\vec{j} = 0.1736$, whereas $\vec{k} = 0$. These unit normal vectors are shown for the most critical node in the first engaged thread root.
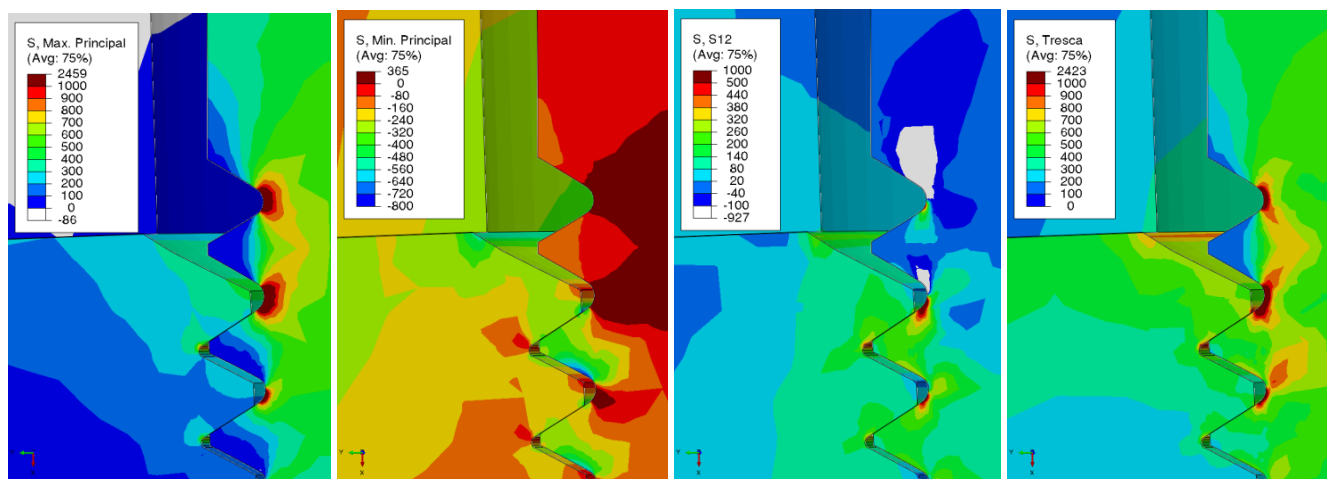
Figure 7. Stress distribution in bolted joint under maximal tensile eccentric force for (a) Max principal, (b) Min principal, (c) shear τ_{xy}, and (d) Tresca stress.

Slika 7. Raspodela napona u vijčanom spoju pod dejstvom maksimalne zatezne ekscentrične sile za (a) glavne zatezne (b) glavne pritisne, (c) smicajne τ_{xy} i (d) Treska napone
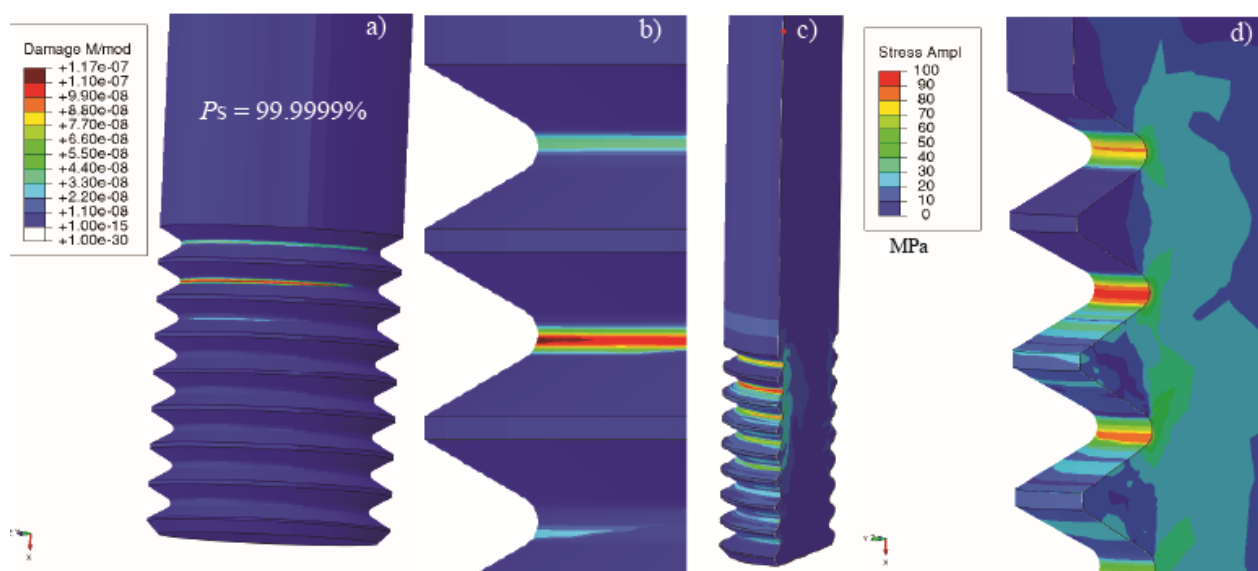

Figure 8. Fatigue damage of model 2 (with 70% of $F_{0.2}$) for P_S = 99.9999%. a) Distribution on bolt, b) distribution in first 3 thread roots, c) stress amplitudes distribution, and d) stress amplitudes distribution in first 3 thread roots.

Slika 8. Zamorno oštećenje modela 2 (sa 70% od $F_{0.2}$ za P_S = 99.9999%. a) Raspodela na vijku, b) raspodela u prva 3 korena navoja, c) raspodela amplituda napona, i d) raspodela amplituda napona u prva 3 korena navoja

Table 2. Model 1 fatigue damage and fatigue strength in dependence of survival probability.

Tabela 2. Zamorno oštećenje i dinamička izdržljivost modela 1 u zavisnosti od verovatnoće preživljavanja

P_S [%]	D [-]	σ_D [MPa]
50	312.16E-09	298
97.5	779.38E-09	249
99	924.72E-09	241
99.9	1.25E-06	225
99.99	1.49E-06	213
99.999	1.73E-06	203
99.9999	1.98E-06	194
99.99999	2.25E-06	186
99.999999	2.53E-06	179

Table 3. Model 2 fatigue damage and fatigue strength in dependence of survival probability.

Tabela 3. Zamorno oštećenje i dinamička izdržljivost modela 2 u zavisnosti od verovatnoće preživljavanja

P_S [%]	D [-]	σ_D [MPa]
50	12.76E-09	228
97.5	31.79E-09	191
99	37.7E-09	185
99.9	53.8E-09	173
99.99	72.11E-09	163
99.999	92.97E-09	155
99.9999	116.72E-09	149
99.99999	143.66E-09	143
99.999999	174.51E-09	138

Table 4. Model 3 fatigue damage and fatigue strength in dependence of survival probability.
Tabela 4. Zamorno oštećenje i dinamička izdržljivost modela 3 u zavisnosti od verovatnoće preživljavanja

| P_S [%]	D [-]	σ_D [MPa]
50	7.41E-09	193
97.5	18.43E-09	162
99	21.86E-09	157
99.9	31.18E-09	146
99.99	41.77E-09	138
99.999	53.84E-09	132
99.9999	67.57E-09	126
99.99999	83.14E-09	121
99.999999	100.97E-09	117

Table 5. Model 4 fatigue damage and fatigue strength in dependence of survival probability
Tabela 5. Zamorno oštećenje i dinamička izdržljivost modela 4 u zavisnosti od verovatnoće preživljavanja

P_S [%]	D [-]	σ_D [MPa]
50	14.29E-06	480
97.5	24.45E-06	402
99	27.03E-06	389
99.9	33.33E-06	363
99.99	39.6E-06	343
99.999	45.99E-06	327
99.9999	52.59E-06	313
99.99999	59.43E-06	300
99.999999	66.64E-06	289

The S-N curve at thread root has a modification from basic material in slope from $k = 12$ at $N_D = 2\cdot10^6$ cycles to $k' = 3.1$ at $N_D = 4.06\cdot10^5$ cycles. The thread root transition in slope is from $k = 3.1$ to $k' = 5.2$ at $N_D = 4.06\cdot10^5$ cycles for cumulative damage calculation, as shown in Fig. 11. R1 position indicates the thread root, F1 indicates right thread flank position which is on tensile side, whereas F2 indicates the left thread flank which is on the compression side due to the contact with nut thread flank. As can be seen in Fig. 11 for F1 and F2, local S-N curve slopes are $k = 5.2$ and $k = 4$, respectively. However, at bolt shank, the S-N curve has a transition in slope from $k = 9.4$ to $k' = 17.8$ at $N_D = 1.76\cdot10^6$ cycles, as shown in Fig. 12. Steeper slopes at thread roots

are caused with the high stress gradients and mean stress, whereas at bolt shank the stress gradients are very small which result with shallower slope. The slope at bolt shank is shallower due to the influence from mean stresses only.
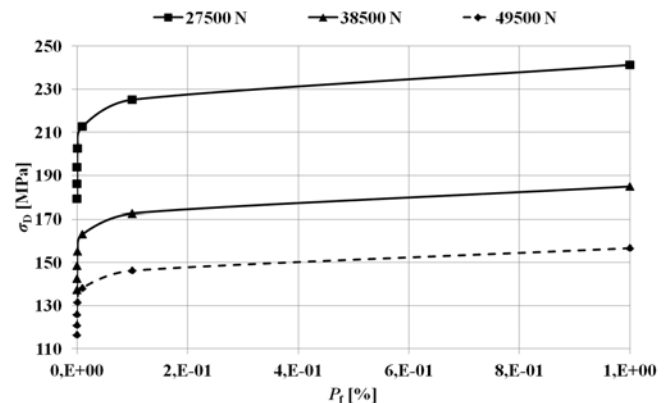
Figure 9. Fatigue strength in dependence of failure probability P_f for models with 50%, 70%, and 90% of $F_{0.2}$.
Slika 9. Dinamička izdržljivost u zavisnosti od verovatnoće otkaza P_f za modele sa 50%, 70%, i 90% od $F_{0.2}$

The stress gradient influence on slope of the local S-N curve ($f_{GR,sf}$) and mean stress influence ($f_{\sigma M,sf}$) are evaluated to investigate the dominant influence on S-N curve slope at first engaged thread root. Results are shown in Table 6. Influence of stress gradients on S-N curve slope is slightly decreased for higher preloads. From $f_{GR,sf} = 22.4$ at preload force of $F_P = 27500$ N, to $f_{GR,sf} = 21.1$ at preload force of $F_P = 49500$ N. However, on the other hand, the mean stress influence on local S-N curve slope has increased due to higher preload forces. From $f_{\sigma M,sf} = 1.8$ at $F_P = 27500$ N, to $f_{\sigma M,sf} = 3.4$ at $F_P = 49500$ N.

Influence of stress gradients (χ) on S-N curve slope at first engaged thread root is shown in Table 7. With χ influence slope is $k = 3.1$, whereas without χ influence $k = 11.1$ for first 3 models with preload forces. The model 4 with χ influence result in slope of $k = 3$, whereas without χ influence $k = 11$. The S-N curve slope for bolt shank is $k = 9.4$ and $k = 10.9$ without stress gradient influence.
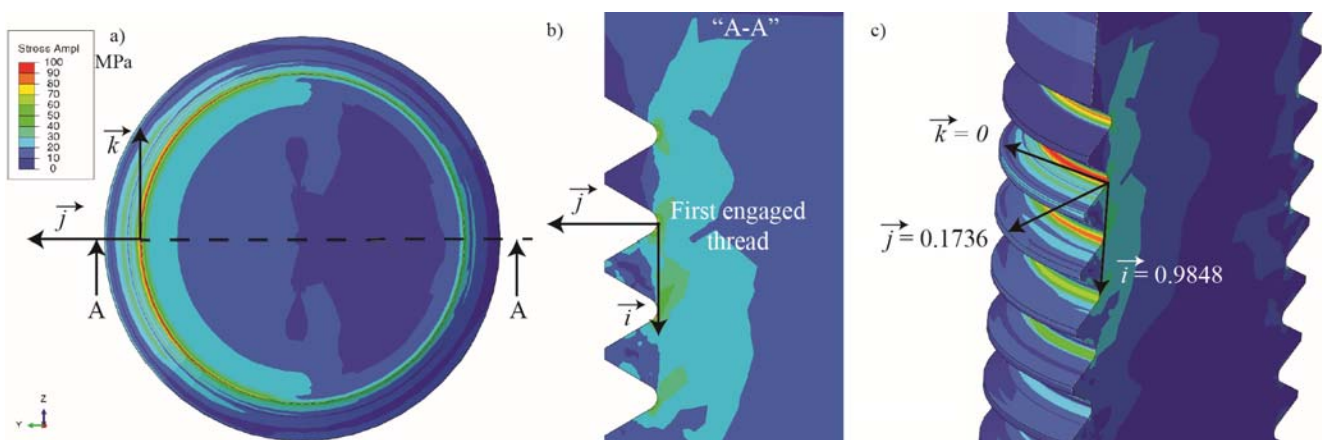

Figure 10. Unit normal vectors of critical cutting plane for crack initiation: a) top view of first engaged thread root, b) and c) section view.
Slika 10. Jedinični normalni vektori kritične ravni za inicijaciju prsline: a) pogled odozgo prvog korena u zahvatu, b) i c) poprečni presek
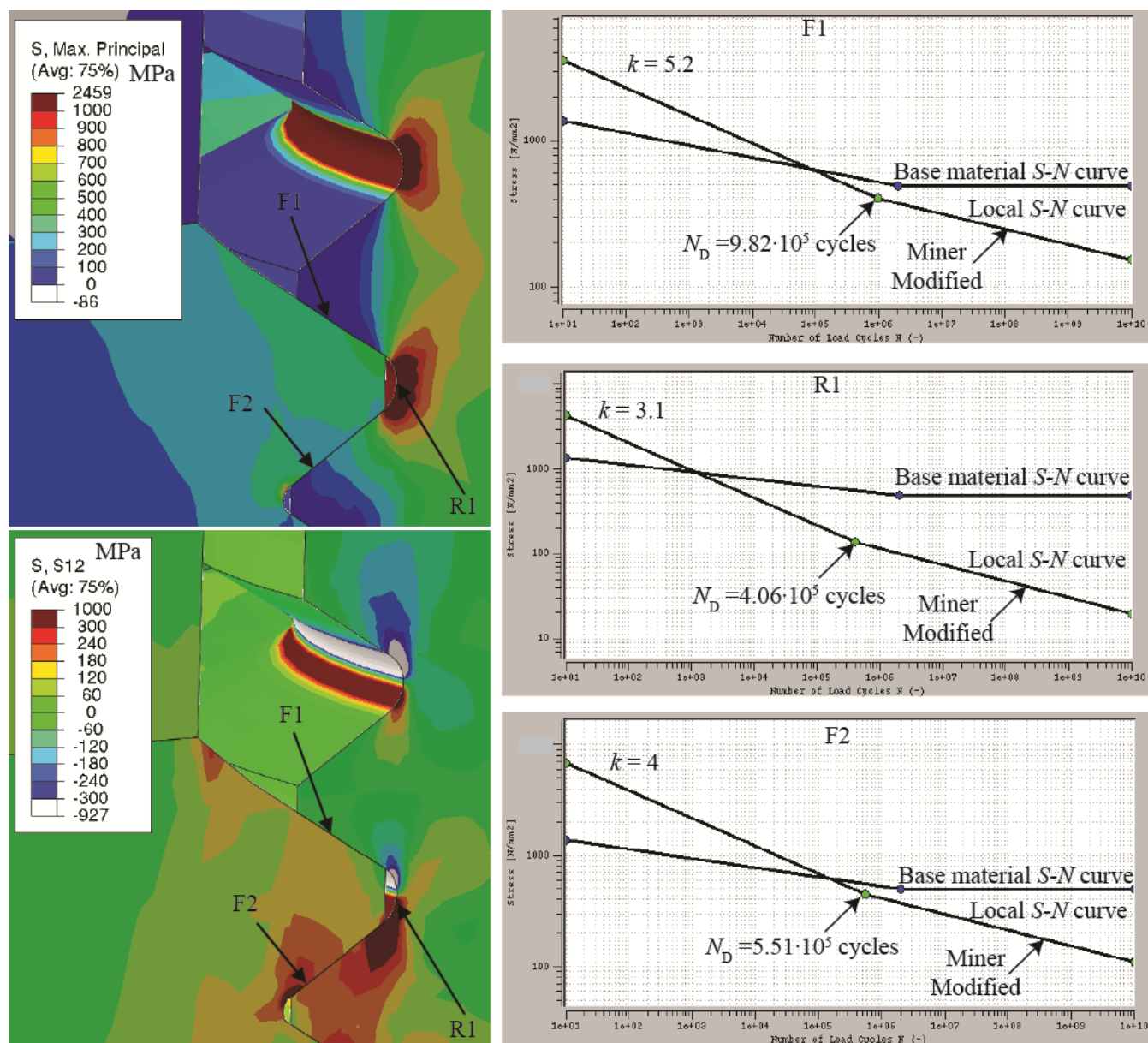
Figure 11. Local S-N curves for thread root and thread flanks.
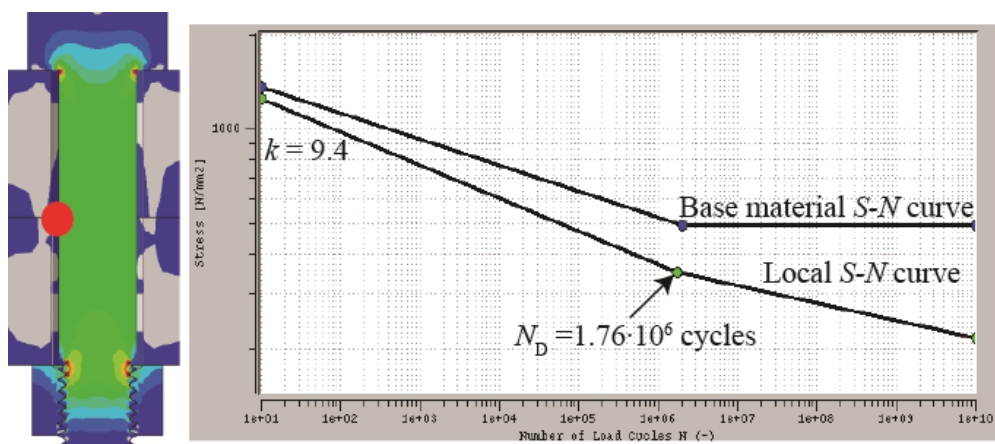Slika 11. Lokalne S-N krive za koren navoja i bokove navoja

Figure 12. Local S-N curve for bolt shank.
Slika 12. Lokalna S-N kriva za telo vijka

Table 6. Stress gradient ($f_{GR,sf}$) and mean stress ($f_{\sigma M,sf}$) influence on local S-N curve slope at first engaged thread root.

Tabela 6. Uticaji gradijenata napona ($f_{GR,sf}$) i srednjih napona ($f_{\sigma M,sf}$) na nagib lokalne S-N krive u prvom korenu navoja u zahvatu

F_P [N]	$f_{GR,sf}$	$f_{\sigma M,sf}$
27500	22.4	1.8
38500	21.8	2.7
49500	21.1	3.4
0	22.8	1.0

Table 7. Influence of stress gradients on S-N curve slope at first engaged thread root.

Tabela 7. Uticaji gradijenata napona na nagib lokalne S-N krive u prvom korenu navoja u zahvatu

F_P [N]	k [-] with χ influence	k [-] without χ influence
27500	3.1	11.1
38500	3.1	11.1
49500	3.1	11.1
0	3.0	11

As can be seen from results, with increase of survival probability the fatigue strength is significantly decreased, especially for very high reliability. One of the most important influence on fatigue damage of bolted joint is stress gradient which has led to much steeper local S-N curves.

DISCUSSION

These results, based on FE and fatigue damage analyses with stress based critical plane approach, have shown that the most critical fatigue point is at the first engaged thread root, which matches results from literature /8, 21, 80-85/.

Furthermore, the results are in accordance with experimental results for the S-N curve slope and knee point. This investigation shows that on the most critical thread root position, the obtained slope is $k = 3.1$ and number of cycles $N_D = 4.06 \cdot 10^5$. A comprehensive literature overview for steels according to Hück et al. /86/, shows the average decrease in the slope of $k = 12.5$ for $K_t = 1$ on $k = 4$ for $K_t = 8$. The number of cycles in the knee point of the S-N curve was shifted from $N_D = 2 \cdot 10^6$ to $N_D = 4 \cdot 10^5$ for $k = 3$. Mostly for steel smooth specimen $k \approx 15$, whereas for a structure with notches $k \approx 5$ and in the case that a sharp notch is present, $k \approx 3$, /58/. For welded joints in general, $k = 3–4$. In the case when the nominal stress method is used with normal stress, the slope is $k = 3.0$. Slopes of $k = 3$ are according to IIW recommendations, /87/. As valid for welded joints regarding the S-N curve slope k, the similar can be applied for bolted or threaded joints in general. However, according to Sonsino /88/, the slope depends on the loading mode (axial, bending, torsion, stress ratio), geometry, stiffness, stress concentration and, in consequence, on the ratio between crack propagation and total life. The slope beyond the knee point results from linear regression analyses and curve fitting. Moreover, in the case of welded joints, the knee point additionally depends on the magnitude of residual stresses /89, 90/. In general, with an increase of notch sharpness, the slope k becomes steeper and the number of cycles at the fatigue limit N_D decreases in the S-N curve.

Generally speaking, fatigue assessment is usually done with nominal stress approach from Eurocode 3 /26/ or VDI 2230 /27/. Eurocode 3 provides a unique (rough) limit of stress amplitude at $2 \cdot 10^6$ cycles equal to $\sigma_A = 25$ MPa. VDI 2230 applies to steel bolts (threads with 60° flank angle), strength classes 8.8 to 12.9, and is recommended for bolt diameters smaller than 40 mm. The load can consist of static and/or dynamic axial loads, whereas bending moments and transverse loads may occur. VDI 2230 recommends for the most critical joints to verify calculation results with experimental or numerical investigations. In the case of Eurocode 3 the relevant S-N curve detail category 50 is not verified for bolt diameters larger than 36 mm, /91/.

Fatigue strength for bolted joints is more conservative in EC3 than in VDI 2230 /91/. According to VDI 2230, if numbers of alternating cycles are $N_D = 2 \cdot 10^6$, then for the stress amplitude of the thread fatigue limit, which is rolled before heat treatment or rolled after heat treatment, can be calculated with the following equations, respectively.

$$\sigma_{ASV} = 0.85(150/d + 45) \tag{20}$$

$$\sigma_{ASG} = (2 - F_{Sm}/F_{0.2min})\sigma_{ASV} \tag{21}$$

where d is the diameter of the bolt, F_{Sm} is the average bolt load, and $F_{0.2min}$ is the bolt load at the minimum yield point. The values for the fatigue limit are related to the stress cross section A_S according to DIN 969 and ISO 3800, of high-strength bolts according to DIN EN ISO 898-1 with standard threads 6g/6H. Only Eq.(21) for fatigue limit of thread which is rolled after heat treatment is preload dependent.

Moreover, bolted joints can be assessed with DNV-RP-C203, /92/. According to DNV-RP-C203, connections where the pretensioned bolts are subjected to dynamic axial forces should be designed with respect to fatigue, taking into account the stress range in the bolts. Accordingly, fatigue assessment in the HCF region is for bolts and threaded rods in tension as well as bolts in single or double shear. DNV-RP-C203 detail category for cold rolled threads with no following heat treatment is F1, whereas for cut threads detail category is W3. F1 and W3 correspond to the notation of 63 and 36, respectively in Eurocode 3 and IIW. It can be seen that cut threads correspond to the worst case of welded joint. According to DNV-RP-C203, stress response from wave action shows typically $5 \cdot 10^6$ cycles.

Additionally, unfired pressure vessels standard BS EN 13445-3:2009 /93/ include bolted joints fatigue assessment. Fatigue limit can be calculated as $\Delta\sigma_D/R_m = 0.0522$ at $2 \cdot 10^6$ cycles and is used for any thread form (machined, ground or rolled) for failure probability of $P_f = 0.1\%$.

Besides previously mentioned engineering fields of general application, high pressure equipment and offshore structures, safe design of bolted joints is additionally very important in transportation and hoisting equipment, where special safety regulations must be fulfilled. For instance, according to the safety standards of the Nuclear Safety Standards Commission (KTA) for the design of lifting equipment in nuclear power plants /94/ the stress analysis shall be performed with respect to the VDI 2230 guidelines for bolted joints where the yield stress during tightening is

limited to 70% and safety factor of 2.0 against the stress amplitude of the endurance shall be satisfied.

Fatigue of threaded joints is different from general structural fatigue problems because of the various influence factors and in-service conditions in a variety of industrial applications. Fatigue assessment of bolted joints is a typical fatigue problem with a multitude of parameters and influencing factors which have an influence on bolted joint fatigue strength. Fatigue damage results from the combined effect of a large number of influence factors. Nominal approaches do not take into account complex thread geometry with blunt notches, nonlinear contact interactions, and cannot consider local stress-strain state at the thread root which results without an accurate thread notch effect. For the nominal approach, stress is really simple because it is just the average stress in the bolt cross-section in an ideally cylindrical bolt joint. To consider and describe local stress-strain state in thread root with realistic notch effect, stress gradients, remarkable mean stress introduced during tightening, stress amplitudes, and damage accumulation can only be estimated by the local method. Nevertheless, fatigue assessment is a complex task due to the significant number of uncertainties that are inherent to the fatigue phenomenon /95-97/. Threaded joints have several peculiarities that complicate fatigue damage assessments. This statement, however, holds true at least as far as an attempt is made to take all the details and influence factors into account for fatigue assessment. The number of influencing parameters is large, but can be summarized for the local approach. The main difficulties encountered in threaded joint fatigue damage assessment are due to uncertainties in accurately defining the following:

1. material monotonic/cyclic properties, local S-N curve, and Haigh diagram,
2. production aspects (surface quality, residual stresses, hardness, etc.),
3. thread profile geometry and tolerances,
4. uncertainties regarding the coefficient of friction,
5. uncertainties in the scatter of preload force and dynamic loads spectra,
6. uncertainties in the Palmgren-Miner damage summation rule, and
7. in environmental influences.

Mechanical properties can be quite different throughout the threaded joint due to production and surface treatments. The thread profile geometry within appropriate tolerance class may vary in reality since many dimensional parameters exist (pitch, major and minor diameter, height of thread profile, root radius, etc., and their relationship).

All these parameters are usually very small and include complex thread details like thread root radius with blunt notches and thread flanks which on the other hand have nonlinear contact interactions. Thread blunt notches with small root radius and application of coarse or fine threads which have different root radius results with different fatigue response. Thread flank contact surfaces experience slippage and they are subjected to contact forces due to pressure and friction which result in thread bending. This in turn results with high stress concentrations and stress gradi-

ents in thread roots. Only the local approach has a potential with sensitivity analysis to improve fatigue behaviour of the particular structure. Nominal approach without detailed geometry of thread roots and influence factors cannot give answers related to details where fatigue cracks initiate. Furthermore, high strength steels provide higher fatigue strength, but they are significantly more notch sensitive. In this case, thread notches are more detrimental than in low strength steels. Scatter of the preload force depends on the tightening approach which in some cases has a high scatter (e. g., tightening with impact wrench or impact wrench with momentum control up to ±60%, torque-controlled tightening up to ±43%, yield-controlled tightening up to ±17%, elongation-controlled tightening with ultrasound ±10%). Hydraulic tensioners have significantly lower scatter which is usually from ±5% up to ±10%. Hydraulic tensioners are commercially available for a variety of engineering applications as wind turbines, pump heads, engine cylinder heads, foundation bolt connections, etc. In addition, special applications as subsea tensioners are also available. Highest accuracy of ±1% can be achieved with the usage of strain gauges. Special nuts are also developed, as for instance, a hydraulic nut which is an internally threaded annular jack. All these uncertainties are directly related to the threaded joint reliability and safety. Threaded joint integrity is the key basis of safe and leak-free operations and tightening is one of the key factors related to the bolted joint integrity. For many applications, stress history due to dynamic loadings can only be made with approximate estimations. For some fields of application, standardised load histories are given by a regulation or code. For instance, WASH for offshore structures (structural members of oil platforms), WISPER for wind turbines, WAWESTA for drive train components, Gaussian load distributions with narrow-band, medium-band, and wide-band random sequence, and many others. Statistical data for fatigue and cyclic properties is mostly coming from laboratory experimental investigations, not from real in-service conditions. This is very important for environment conditions. These all peculiarities change over time. The first microcrack growth is a surface phenomenon where a various number of influences are present. Surface roughness, surface treatments and layers are of particular significance and influence on crack initiation phase since fatigue cracks initiate on the surface. These surface conditions have no particular influence on crack growth because crack growth is a matter of material bulk properties, /98/. According to Schijve /98/, material and surface finishing effects on scatter/range of dispersion are similar on both specimen and real structures. The failure initiates always at the surface (also at a very high number of cycles), which is caused by high stress concentration in the thread root. The crack initiation site for smooth specimens at a higher number of cycles (approximately $N > 7 \cdot 10^6$) is always below the surface at a distance between several 10 µm to 1 mm, /81/. The number of influence factors significantly increases when the approach is switched from nominal to local approach. This in turn requires excessive detailed modelling and knowledge of a variety of influence factors.

The fatigue damage D theoretically equals 1.0 at fatigue failure. However, in reality and engineering practice due to the uncertainties related to the proportional and non-proportional loadings, stress multiaxiality, fabrication, and other errors, the value of D is usually less than 1. About 90% of all experimental results are below 1, /99/. According to FKM-Guidelines /58/, the critical damage sum for non-welded steel components is $D_M = 0.3$.

The discussion above shows that generally, the standard nominal approach can be used as a first guideline for dimensioning, from which further design improvement based on local approaches may originate. The potential of the local approach lies in the fact that only local approach takes into account the influence factors and detailed geometry which have a decisive influence on the fatigue behaviour and lifetime.

The safety margin and the influence of each influence factor on structural reliability are significantly valuable knowledge for structural integrity. Expensive interventions and the demand for higher safety and environmental protection have increased the need for higher reliability of bolted joints, /3/.

Determination of the fatigue limit of threads is relevant for considering the risk of fatigue crack initiation in in-service structures, especially for large structures with complex loading which must accomplish a high reliability of structural integrity.

If regular in-service monitoring is not specified, the survival probability must be high, /87/. High uncertainties are associated with fatigue damage assessment. These high uncertainties associated with fatigue damage imply that in-service inspection for fatigue cracks will be required during life depending on the consequence of a fatigue failure and estimated fatigue damage/life. Certain reliability depends on the consequence and nature of failure. Uncertainty modelling for target reliability level in offshore is according to /100/, with a value of failure probability $P_f = 10^{-6}$ for a serious consequence when the class of failure has no warning before the occurrence of failure.

According to DNV-RP-C-203, /92/: if the consequence of a fatigue crack is substantial the accumulated probability of fatigue failure should be less than 10^{-4} and an inspection would be required after 2 years. After a first inspection the time interval to the next inspection can be estimated based on fracture mechanics and probabilistic analysis taking into account the uncertainty in the inspection method.

According to DNV-OS-C101, /101/, design fatigue factors (DFF) shall be applied to reduce fatigue failure probability (P_f). These factors are dependent on the significance of structural components with respect to structural integrity and availability for inspection and repair. DFF has a maximum value of 3 for non-accessible areas, areas not planned to be accessible for inspection and repair during operation. For instance, welds beneath positions 150 m below water level and splash zone should be assumed inaccessible for in-service inspection. Units intended to follow normal inspection schedule according to class requirements, i.e. the 5-year inspection interval in sheltered waters or drydock, may apply a Design Fatigue Factor (DFF) of 1.

According to DNV-OS-C101, the S-N curves shall be based on a survival probability of $P_S = 97.6\%$, corresponding to the mean minus-two-standard-deviation curves of relevant experimental data. IIW-Recommendations /87/ require that the prerequisites for allowable stress ranges for welded joints must be derived for $P_s = 97.7\%$. The allowable equivalent stress ranges for $P_s = 97.7\%$ are derived based on Gaussian log-normal distribution with a scatter of $T_S = 1.50$ for welded joints. Therefore, fatigue strength properties are usually given with ±1 up to 3 standard deviations. From engineering standards, the accepted survival probability or failure probability depends on the consequences of failure with target reliability levels.

These values of fatigue limits in thread roots also need to be determined based on experiments. However, experiments are extremely hard to apply on thread roots due to very small dimensions. For instance, thread root radius on used bolt M10 with normal threads is only $r = 0.217$ mm. Therefore, from authors' knowledge, all experiments on bolted joints are done with nominal approach, with stresses in bolt stress cross section.

It is the authors' opinion that threaded joints have a large number of significant influence factors and peculiarities affecting the fatigue behaviour and fatigue damage, and trying to predict damage with high accuracy on a single numerical model is quite hard. Moreover, a lack of information in service is always present. But, this study shows how tightening forces and survival probability influence the fatigue damage, which gives useful information for engineering practice. The target of fatigue damage analysis should be to ensure that the probability of fatigue failure and consequences of this failure be in the safety range for risk and economic significance.

Furthermore, it is the authors' opinion that with the acceptance of all uncertainties related to fatigue, statistics and probability should be applied for threaded joint integrity. Concentration on influence factors which have the highest influence and are also decisive is the most important basis for the reliable application of local approach.

Conclusively, fatigue damage and structural integrity of bolted joints can be determined only with certain probability of survival or failure. Due to the significant survival probability influence on fatigue damage, in-service inspection for fatigue cracks will be required during life depending on the consequence of a fatigue failure and estimated fatigue damage, because connection between assessment of fatigue damage and in-service inspection is mandatory.

CONCLUSIONS

The most important conclusion to be drawn here is that fatigue damage and the fatigue limit for a specific number of cycles can be determined only with certain probability of survival or failure. Nevertheless, under the parameters of FE and fatigue damage analyses with influence factors, statistics, and probability in this study, the following conclusions are drawn concerning the fatigue in dependence of survival probability:
- increase of bolt preload force up to 90% of $F_{0.2}$ results with lower fatigue damage, whereas the fatigue limit

decreases. On the other hand, with increase of preload force, maximal stress amplitude decreases. It has a beneficial effect on fatigue damage. The model without preload force has the highest fatigue damage, whereas the model with 90% of $F_{0.2}$ has minimal fatigue damage,

- fatigue strength has a significant decrease for lower failure probabilities and therefore, statistics and probability have a very significant influence on fatigue damage and fatigue strength,

- Steeper slopes at thread root with $k = 3.1$ are caused by high stress gradients and mean stresses, whereas at bolt shank the stress gradients are very small which results in shallower slope of $k = 9.4$. Thread flanks on compressive side have slope of $k = 4$, whereas on the tensile side the slope is $k = 5.2$. In general, with an increase of the notch sharpness, the slope k becomes steeper and the number of cycles at the fatigue limit N_D decreases in the S-N curve,

- Nominal approach can be used as a first guideline for dimensioning, from which further design improvement based on local approaches may originate. The number of influence factors significantly increases when the approach is switched from nominal to local approach,

- Determined fatigue damage and/or fatigue life should form the basis for efficient and safe in-service inspection time intervals as well as inspection during manufacture.

ACKNOWLEDGEMENT

REFERENCES

1. Schijve, J., *Fatigue of Structures and Materials in the 20th Century and the State of the Art*, Int J Fatigue, Vol.25, pp.679-702, (2003).

2. Schijve, J., *The significance of fatigue crack initiation for predictions of the fatigue limit of specimens and structures*, Int J Fatigue, Vol.61, pp.39-45, (2014).

3. Esaklul, K.A., Ahmed, T.M., *Prevention of failures of high strength fasteners in use in offshore and subsea applications*, Eng Fail Anal, Vol.16, pp.1195-1202, (2009).

4. Sungkon, H., *Fatigue analysis of drillstring threaded connections*, Proceedings of The Thirteenth International Offshore and Polar Engineering Conference Honolulu, Hawaii, USA, May 25-30, pp.202-208, (2003).

5. Shahani, A.R., Sharifi, S.M.H., *Contact stress analysis and calculation of stress concentration factors at the tool joint of a drill pipe*, Mater Design, Vol.30, pp.3615-3621, (2009).

6. Ferjani, M., Averbuch, D., Constantinescu, A., *A computational approach for the fatigue design of threaded connections*, Int J Fatigue, Vol.33, pp.610-623, (2011).

7. Hill, T.H., *A unified approach to drillstem failure prevention*, SPE Drill Eng, Vol.7, pp.254-260, (1992).

8. Tafreshi, A., Dover, W.D., *Stress analysis of drillstring threaded connections using the finite element method*, Int J Fatigue, Vol.15, pp.429-38, (1993).

9. Bertini, L., Beghini, M., Santus, C., Baryshnikov, A., *Resonant test rigs for fatigue full scale testing of oil drill string connections*, Int J Fatigue, Vol.30, pp.978-88, (2008).

10. Ciavarella, M., Meneghetti, G., *On fatigue limit in the presence of notches: classical vs. recent unified formulations*, Int J Fatigue, Vol.26, pp.289-98, (2004).

11. Susmel, L., Taylor, D., *Two methods for predicting the multiaxial fatigue limits of sharp notches*. Fatigue Fract Eng Mater Struct, Vol.26, pp.821-33, (2003).

12. Naik, R.A., Lanning, D.B., Nicholas, T., Kallmeyer, A.R., *A critical plane gradient approach for the prediction of notched HCF life*, Int J Fatigue, Vol.27, pp.481-92, (2005).

13. Hofmann, F., Bertolino, G., Constantinescu, A., Ferjani, M., *A multiscale discussion of fatigue and shakedown for notched structures*, Theor Appl Fract Mech, Vol.48, pp.140-51, (2007).

14. Hofmann, F., Bertolino, G., Constantinescu, A., Ferjani, M., *A discussion at the mesoscopic scale of the stress-gradient effects in high cycle fatigue based on the Dang Van criterion*, J Mech Mater Struct, Vol.4, pp.293-308, (2009).

15. Fares, Y., Chaussumier, M., Daidie, A., Guillot, J,. *Determining the life cycle of bolts using a local approach and the Dang Van criterion*, Fatigue Fract Eng Mater Struct, Vol.29, pp.588-96, (2006).

16. McEvily, A.J., Atlas of Stress Corrosion and Corrosion Fatigue Curves, ASM International, 1990.

17. Bickford, J.H., An introduction to the design and behavior of bolted joints. 2nd Ed. Marcel Deckker, 1990.

18. ASME/ANSI B16 – standards of pipes and fittings, 2003.

19. API Spec 6A, Specification for wellhead and christmas tree equipment. Washington DC, American Petroleum Institute, 2004.

20. Review of Repairs to Offshore Structures and Pipelines, Publication 94/102, Marine Technology Directorate, UK, 1994.

21. Cho, S.S., Chang, H., Lee, K.W., *Dependence of fatigue limit of high-tension bolts on mean stress and ultimate tensile strength*, Int J Automot Techn, Vol.10, pp.475-479, (2009).

22. Johnston, T.L., Karaikovic, E.E., Lautenschlager, E.P., Marcu, D., *Cervical pedicle screws vs. lateral mass screws: uniplanar fatigue analysis and residual pullout strengths*, Spine J, Vol.6, pp.667-672, (2006).

23. Brasiliense, L.B.C., Lazaro, B.C.R., Reyes, P.M., Newcomb, A.G.U.S., Turner, J.L., Crandall, D.G., Crawford, N.R., *Characteristics of immediate and fatigue strength of a dual-threaded pedicle screw in cadaveric spines*, Spine J, Vol.13, pp.947-956, (2013).

24. Novoselac, S., Ergić, T., Kozak, D., Sertić, J., Pacak, M., *Influence of dental implant screw preload force on high-cycle fatigue* (in Croatian), Proceedings of 5th Croatian Society of Mechanics, ed. I. Karšaj, T. Jarak, Donja Stubica, Croatia, 6-7 June 2013, pp.137-142.

25. Novoselac, S., Ergić, T., Kozak, D., Baškarić, T., *Structural durability of dental implants* (in Croatian), Proceedings of 6th Croatian Society of Mechanics, ed. G. Jelenić, M. Gaćeša, Rijeka, Croatia, 29-30 May 2014, pp.251-256.

26. Eurocode No. 3: Design of steel constructions, Part 1. Beuth-Verlag, Berlin; 1993.

27. Verein Deutscher Ingenieure, VDI 2230 Guidelines, 2003.

28. Schneider, R., Wuttke, U., Berger, C., *Fatigue Analysis of Threaded Connections Using the Local Strain Approach*, Procedia Eng, Vol.2, pp.2357-2366, (2010).

29. Dixon, D.L., Breeding, L.C., Sadler, J.P., McKay, M.L., *Comparison of screw loosening, rotation, and deflection among three implant designs*, J Prosthet Dent, Vol.74, pp.270-8, (1995).

30. Patterson, E.A., Kenny, B., *A modification to the theory for the load distribution in conventional nuts and bolts*, J Strain Anal Eng Des, Vol.21, pp.17-23, (1986).

31. Sopwith, D.G., *The distribution of load in screw threads*, Inst Mech Eng Proc, Vol.159, pp.373-383, (1948).

32. D'Eramo, M., Cappa, P., *An experimental validation of load distribution in screw threads*, Exp Mech, Vol.31, pp.70-75, (1991).

33. Kenny, B., Patterson, E., *Load and stress distribution in screw threads*, Exp Mech, Vol.25, pp.208-213, (1985).

34. Wang, W., Marshek, K.M., *Determination of load distribution in a threaded connector with yielding threads*, Mech Mach Theory, Vol.31, pp.229-244, (1996).

35. Croccolo, D., Agostinis, M., Vincenzi, N., *A contribution to the selection and calculation of screws in high duty bolted joints*, Int J Press Vessels Pip, Vol.96-97, pp.38-48, (2012).

36. Griza, S., da Silva, M.E.G., dos Santos, S.V., Pizzio, E., Strohaecker, T.R., *The effect of bolt length in the fatigue strength of M24x3 bolt studs*, Eng Fail Anal, Vol.34, pp.397-406, (2013).

37. Patterson, E.A., *A comparative study of methods for estimating bolt fatigue limits*, Fatigue Fract Eng Mater Struct, Vol.13, pp.59-81, (1990).

38. Fares, Y., Chaussumier, M., Daidie, A., Guillot, J., *Determining the life cycle of bolts using a local approach and the Dang Van criterion*, Fatigue Fract Engng Mater Struct, Vol.29, pp.588-596, (2006).

39. Liao, R., Sun, Y., Liu, J., Zhang, W., *Applicability of Damage Models for Failure Analysis of Threaded Bolts*, Eng Fract Mech, Vol.78, pp.514-524, (2011).

40. Susmel, L., Tovo, R., *Estimating fatigue damage under variable amplitude multiaxial fatigue loading*, Fatigue Fract Engng Mater Struct, Vol.34, pp.1053-1077, (2011).

41. Łagoda, T., Macha, E., *Estimated and experimental fatigue lives of 30CrNiMo8 steel under in-and out-of-phase combined bending and torsion with variable amplitude*, Fatigue Fract Eng Mat Struct, Vol.11, pp.1307-1318, (1994).

42. Morel, F., *A critical plane approach for life prediction of high cycle fatigue under multiaxial variable amplitude loading*, Int J Fatigue, Vol.22, pp.101-119, (2000).

43. Carpinteri, A., Spagnoli, A., Vantadori, S., *A multiaxial fatigue criterion for random loading*, Fatigue Fract Eng Mat Struct, Vol.26, pp.515-522, (2003).

44. Łagoda, T., Ogonowski, P., *Criteria of multiaxial random fatigue based on stress, strain and energy parameters of damage in the critical plane*, Mat-wiss u Werkstofftech, Vol.36, pp.429-437, (2005).

45. Marciniak, Z., Rozumek, D., Macha, E., *Fatigue lives of 18G2A and 10HNAP steels under variable amplitude and random non-proportional bending with torsion*, Int J Fatigue, Vol.30, pp.800-813, (2008).

46. Matake, T., *An explanation on fatigue limit under combined stress*, Bull JSME, Vol.20, pp.257-263, (1977).

47. McDiarmid, D.L., *A shear stress based critical-plane criterion of multiaxial fatigue failure for design and life prediction*, Fatigue Fract Eng Mater Struct, Vol.17, pp.1475-1484, (1994).

48. Susmel, L., Lazzarin, P., *A bi-parametric modified Wöhler curve for high cycle multiaxial fatigue assessment*, Fatigue Fract Eng Mater Struct, Vol.25, pp.63-78, (2002).

49. Susmel, L., Petrone, N., *Multiaxial fatigue life estimations for 6082-T6 cylindrical specimens under in-phase and out-of-phase biaxial loadings*, In: Biaxial and Multiaxial Fatigue and Fracture, (Eds. A. Carpinteri, M. de Freitas and A. Spagnoli), Elsevier and ESIS, Oxford, UK, pp.83-104, (2003).

50. Lazzarin, P., Susmel, L., *A stress-based method to predict lifetime under multiaxial fatigue loadings*, Fatigue Fract Eng Mater Struct, Vol.26, pp.1171-1187, (2003).

51. Forsyth, P.J.E., *A two stage process of fatigue crack growth*, In: McDowell DL, editor. Proceedings of the crack propagation symposium, Cranfield, pp.76-94, (1961).

52. Jahed, H., Varvani-Farahani, A., *Upper and lower fatigue life limits model using energy-based fatigue properties*, Int J Fatigue, Vol.28, pp.467-473, (2006).

53. Zhang, G., *Method of effective stress for fatigue: Part I - A general theory*, Int J Fatigue, Vol.37, pp.17-23, (2012).

54. Novoselac, S., Kozak, D., Ergić, T., Šimić, I., *Influence of Stress Gradients on Bolted Joint Fatigue Behaviour Under Different Preloads and Cyclic Loads Ratio*, Structural Integrity and Life, Vol.14, pp.3-16, (2014).

55. Chen, J.J., Shih, Y.S., *A study of the helical effect on the thread connection by three dimensional finite element analysis*, Nucl Eng Des, Vol.191, pp.109-116, (1999).

56. Haibach, E., Betriebsfestigkeit: Verfahren und Daten zur Bauteilberechnung. 3rd Ed. Berlin, Springer-Verlag, (2006).

57. Wiegand, H., Kloos, K.H., Thomala, W., Schraubenverbindungen: Grundlagen, Berechnung, Eigenschaften, Handhabung. 5. Auflage. Springer-Verlag Berlin, (2007).

58. Forschungskuratorium Maschinenbau (FKM). Analytical strength assessment of components in mechanical engineering, 5th Ed. VDMA Verlag GmbH, (2003).

59. ECS Steyr. FemFat 4.7: Theory Manual. St. Valentin, (2007).

60. Pyttel, B., Schwerdt, D., Berger, C., *Very high cycle fatigue - Is there a fatigue limit?* Int J Fatigue, Vol.33, pp.49-58, (2011).

61. Karolczuk, A., Macha, E., *Critical and fracture plane orientations under multiaxial cyclic and random loading*, Arch Mech Eng, Vol.51, pp.415-35, (2004).

62. Karolczuk, A., Macha, E., Critical planes in multiaxial fatigue of materials, monograph. Fortschritt-Berichte VDI, Mechanik/ Bruchmechanik, reihe 18, nr. 298. Dusseldorf, VDI Verlag, pp.204, (2005).

63. Karolczuk, A., Macha, E., *Critical planes in multiaxial fatigue*, Mater Sci Forum, Vol.482, pp.109-14, (2005).

64. Karolczuk, A., Macha, E., *A review of critical plane orientations in multiaxial fatigue failure criteria of metallic materials*, Int J Fract, Vol.134, 267-304, (2005).

65. Karolczuk, A., Macha, E., *Selection of the critical plane orientation in twoparameter multiaxial fatigue failure criterion under combined bending and torsion*. Eng Fract Mech, Vol.75, pp.389-403, (2008).

66. Macha, E., Niesłony, A., *Critical plane fatigue life models of materials and structures under multiaxial stationary random loading: The state-of-the-art in Opole Research Centre CESTI and directions of future activities*, Int J Fatigue, Vol.39, pp.95-102, (2012).

67. Bedkowski, W., Macha, E., *Maximum normal stress fatigue criterion applied to Random Triaxial Stress State*, Theor Appl Fract Mech, Vol.7, pp.89-107, (1987).

68. ECS Steyr. FemFat 4.8: MAX Manual. St. Valentin, (2007).

69. Bathias, C., *There is no infinite fatigue life in metallic materials*, Fatigue Fract Engng Mater Struct, Vol.22, pp.559-565, (1999).

70. Eurocode No. 9 Design of aluminium structures, Part 2. Beuth- Verlag, Berlin, (1998).

71. Sonsino, C.M., *Course of SN-curve especially in the high-cycle fatigue regime with regard to component design and safety*, Int J Fatigue, Vol.29, pp.2246-2258, (2007).

72. Dowling, N., *Fatigue Failure Predictions for Complicated Stress - Strain Histories*, J Mater, Vol.7, pp.71-78, (1972).

73. Endo, T., *Damage Evaluation of Metals for Random or Varying Loading - Three Aspects of the Rainflow Method*, In: Proc. of Symposium on Mechanical Behaviour of Materials. Japan, Society of Materials Science, pp.372-380, (1974).

74. Standard Practice for Cycle Counting in Fatigue Analysis. ASTM Standard E 1049-1090, American Society for Testing and Materials, (1990).

75. Haibach, E., Matschke, C., *Normierte Wöhlerlinien für ungekerbte und gekerbte Formelemente aus Baustahl*, Stahl und Eisen, Vol.101, pp.21-27, (1981).

76. Amstutz, H., Olivier, R., *Fatigue strength of shear loaded welded joints according to the notch stress concept*, Mat-wiss u Werkstofftech, Vol. 42, (2011).

77. Sonsino, C.M., *Effect of residual stresses on the fatigue behaviour of welded joints depending on loading conditions and weld geometry*, Int J Fatigue, Vol.31, pp.88-101, (2009).

78. Eibl, M., Sonsino, C.M., Stand der Technik zur Schwingfestigkeitsberechnung von laserstrahl-geschweißten Dünnblechen aus Stahl. Report 668. Berlin: DVM; pp.155-71, (2001).

79. Eibl, M., Sonsino, C.M., Kaufmann, H., Zhang, G., *Fatigue assessment of laser welded thin sheet aluminium*, Int J Fatigue, Vol.25, pp.719-31, (2003).

80. Majzoobi, G.H., Farrahi, G.H., Habibi, N., *Experimental evaluation of the effect of thread pitch on fatigue life of bolts*, Int J Fatigue, Vol.27, p.189-196, (2005).

81. Berger, C., Pyttel, B., Trossmann, T., *Very high cycle fatigue tests with smooth and notched specimens and screws made of light metal alloys*, Int J Fatigue, Vol.28, p.1640-1646, (2006).

82. Horn, N. J., Stephens, R. I., *Influence of Cold Rolling Threads Before or After Heat Treatment on High Strength Bolts for Different Fatigue Preload Conditions*, Journal of ASTM International, Vol.3, pp.95-115, (2006).

83. Knez, M., Glodež, S., Kramberger, J., *Fatigue assessment of piston rod threaded end*, Eng Fail Anal, Vol.16, pp.1977-1982, (2009).

84. Macdonald, K.A., Deans, W.F., *Stress analysis of drillstring threaded connections using the finite element method*, Eng Fail Anal, Vol.2, pp.1-30, (1995).

85. Knight, M.J., Brennan, F.P., Dover, W.D., *Effect of residual stress on ACFM crack measurements in drill collar threaded connections*, NDT&E Int, Vol.37, pp.337-43, (2003).

86. Hück, M., Thrainer, L., Schütz, W., Berechnung von Wöhler-Linien für Bauteile aus Stahl, Stahlguß und Grauguß, synthetische Wöhler-Linien. VDEh-Bericht ABF 11, (1981).

87. Hobbacher, A., Recommendations for fatigue design of welded joints and components, Doc. IIW-1823-07 (ex-doc. XIII-2151r4-07/XV-1254r4-07), WRC Bulletin 520, Welding Research Council, Inc., New York, (2009).

88. Sonsino, C.M., *A consideration of allowable equivalent stresses for fatigue design of welded joints according to the notch stress concept with the reference radii rref = 1.00 and 0.05 mm*, Welding in the World, Vol.53, pp.64 -75, (2009).

89. Sonsino, C.M., Über den Einfluss von Eigenspannungen, Nahtgeometrie und mehrachsigen Spannungszuständen auf die Betriebsfestigkeit geschweißter Konstruktionen aus Baustählen. Mat-wiss u Werkstofftech, Vol.25, pp.97-109, (1994).

90. Ritter, W., Kenngrßen der Wöhlerlinien für Schweißverbindungen aus Stählen. Inst. für Stahlbau und Werkstoffmechanik der TU Darmstadt Heft 53, Dissertation TU Darmstadt, (1994).

91. Schaumann, P., Marten, F., *Fatigue Resistance of High Strength Bolts with Large Diameters*, Proceedings of the International Symposium for Steel Structures ISSS, 12.-13.03., Seoul, South Korea, pp.1-8, (2009).

92. DNV-RP-C203, Fatigue Design of Offshore Steel Structures. Det Norske Veritas AS, (2011).

93. BS EN 13445-3:2009. Unfired pressure vessels. BSI, (2009).

94. KTA-Geschaeftsstelle c/o BfS, Germany, 2014

95. Svensson, T., *Prediction uncertainties at variable amplitude fatigue*, Int J Fatigue, Vol.19, pp.295-302, (1997).

96. Tovo, R., *On the fatigue reliability evaluation of structural components under service loading*, Int J Fatigue, Vol.23, pp. 587-98, (2001).

97. Echard, B., Gayton, N., Bignonnet, A., *A reliability analysis method for fatigue design*, Int J Fatigue, Vol.59, pp.292-300, (2013).

98. Schijve, J., *Fatigue predictions and Scatter*, Fatigue Fract Engng Mater Struct, Vol.17, pp.381-396, (1994).

99. Sonsino, C.M., *Fatigue testing under variable amplitude loading*. Int J Fatigue, Vol.29, pp.1080-1089, (2007).

100. DNV, Guideline for offshore structural reliability analysis, Det Norske Veritas, REPORT NO. 95-3204, (1996).

101. DNV-OS-C101, Design of offshore steel structures, general (LRFD method). Det Norske Veritas, (2011).

· · · · · ●●●●● · · · ·

XXIII IGF NATIONAL CONFERENCE (1ST International Edition), 22-24 June, 2015, Favignana (TP), Italy

Main topics

Analyt., comput. and physical models; Biomater. and wood fracture and fatigue; Biomech.; Ceramics fracture and damage; Composites; Comput. mechanics; Concrete & rocks; Creep fracture; Damage mechanics; Damage and fracture in materials under dyn. loading; Durability of structures; Environmentally assisted fracture; Failure analysis and case studies; Fatigue - crack growth (all materials); Fatigue resist. of metals; Fatigue of metals – very high cycle; Failure analysis and forensic engng.; Fractography and advanced metallography; Fracture and fatigue at atomistic and molecular scales; Fracture and fatigue testing systems; Fracture under mixed-mode and multiaxial loading; Fracture vs. gradient mech.; Functional gradient materials; Impact & dynamics; Fundamentals of cohesive zone models; History of fracture mech. and fatigue; Innovative alloys; Linear and nonlinear fract. mech.; Materials mechanical behavior and image analysis; Mesomech. of fracture; Micromech. of fracture and fatigue; Multi-physics and multi-scale modelling of cracking in heterogen. materials; Multiscale experiments and modeling; Nanostruct. materials; Nondestructive examination; Physical aspects of brittle fracture; Physical aspects of ductile fracture; Polymers fract. and fatigue; Probabilistic fract. mech.; Reliability and life extension of comp.; Repair and retrofitting: modelling and practical applic.; Sandwiches, joints and coatings; Smart materials; Structural integrity; Temperature effect; Thin films

Deadlines

28.02.2015: Abstracts submission
15.03.2015: Abstracts notification of acceptance
01.05.2015: Papers submission
15.05.2015: Papers notification of acceptance